catalysts

MDPI

Article

Catalytic Behaviour of CuO-CeO_2 Systems Prepared by Different Synthetic Methodologies in the CO-PROX Reaction under CO_2-H_2O Feed Stream

Juan Antonio Cecilia [1], Ana Arango-Díaz [1], Jaasiel Marrero-Jerez [2,3], Pedro Núñez [2,3], Elisa Moretti [4], Loretta Storaro [4] and Enrique Rodríguez-Castellón [1,*]

1 Departamento de Química Inorgánica, Facultad de Ciencias, Universidad de Malaga, 29071 Malaga, Spain; jacecilia@uma.es (J.A.C.); anarango@uma.es (A.A.-D.)
2 Departamento de Química, Universidad de La Laguna, 38200 La Laguna, Tenerife, Spain; jmarjer@ull.es (J.M.-J.); pnunez@ull.edu.es (P.N.)
3 Instituto de Materiales y Nanotecnología, Universidad de La Laguna, 38200 La Laguna, Tenerife, Spain
4 Dipartimento di Scienze Molecolari e Nanosistemi, Università Ca'Foscari Venezia, Via Torino 155/b, 30172 Mestre-Venezia, Italy; elisam@unive.it (E.M.); storaro@unive.it (L.S.)
* Correspondence: castellon@uma.es; Tel.: +34-952-131-873

Academic Editor: Jean-François Lamonier
Received: 10 April 2017; Accepted: 15 May 2017; Published: 18 May 2017

Abstract: CuO-CeO_2 catalysts, with 6 wt % of Cu, have been synthesised by different preparation methods (calcination of nitrate precursors, thermal urea-nitrate combustion, freeze-drying method, using polymethyl metacrylate PMMA microspheres as template and precipitation using NaOH or the decomposition of urea as precipitating agents). The obtained materials have been characterised by X-ray powder diffraction (XRD), scanning electron microscopy (SEM), transmission electron microscopy (TEM), Raman spectroscopy, N_2 adsorption-desorption at −196 °C, H_2 thermoprogrammed reduction (H_2-TPR) and X-ray photoelectron spectroscopy (XPS). The catalysts displayed high dispersion of copper oxide, obtaining CO conversion values of 90–100% at 115 °C in the CO preferential oxidation in excess of hydrogen (CO-PROX) and maintaining this activity even after 48 h of time on stream. The incorporation of CO_2 and H_2O in the feed stream (simulating a PROX unit) caused a decrease in the CO conversion, except for the catalyst synthesised using PMMA microspheres as a template which maintained a CO conversion of 95% at 115 °C. This catalyst exhibits an excellent catalytic performance, also under real operating conditions, thanks to many and concomitant factors, such as the very small CeO_2 particle size (5.6 nm), the surface being rich in copper (atomic ratio Cu/Ce = 0.35) that is easily reducible, and the peculiar morphology and porosity of the material.

Keywords: ceria; CuO; CuO-CeO_2; CO-PROX; PMMA

1. Introduction

The increase of the world population has led to a high demand for environmentally benign energy sources. Among them, fuel cells are sustainable ways to convert chemical into electrical energy with low emission of pollutants. Several fuel cells, such as polymer-electrolyte membrane (PEMFC), alkaline (AFC), phosphoric acid (PAFC), molten carbonate (MCFC), and solid oxide (SOFC) fuel cells are used for different applications, e.g., stationary power for buildings, micro/portable power or distributed generation for remote areas [1]. The PEMFCs possess many attractive features such as low operating temperature, compactness, low weight, long stack life and sustained operation at high current density [2]. They use hydrogen as fuel, which can be obtained from the steam reforming or

auto-thermal reforming of hydrocarbons or alcohols [3–5] in combination with the water gas shift (WGS) reaction, where most CO is removed [6,7].

After the WGS reaction, the concentration of CO is about 1%. However, the Pt anode catalyst of the PEMFC, which operates in the range of 60–120 °C, is prone to be poisoned by CO at low temperature, even at very low CO concentrations (<10 ppm) in the H_2-rich stream [8,9]. Several methodologies have been proposed for CO removal. The main methods are as follows: (a) purification with hydrogen-selective membranes, (b) CO methanation, (c) pressure swing adsorption and (d) preferential oxidation of CO (CO-PROX) [10]. Among them, the CO-PROX reaction is considered the most promising process for selective CO removal in an H_2-rich stream [11]. It has been reported that supported noble metal catalysts, such as Pt, Pd, Ir, Ru or Rh [12–14], or nano-gold catalysts [14–17] are excellent catalysts for the CO-PROX reaction. These catalysts are able to remove CO content below 10 ppm in the reaction temperature range of 60–150 °C using very little noble metal content [12]. Among these noble metals, platinum-based catalysts have achieved a reduction in CO content below 10 ppm using a real feed with H_2, H_2O and CO_2 at 65 °C [18]. However, the high cost, sensitivity to poisoning and sintering at higher temperature of the noble-metal-based catalysts has led to the development of abundant, inexpensive active phases with great resistance to CO_2 and H_2O poisoning [14]. In this sense, CuO-CeO_2 systems have been proposed as promising catalysts for the CO-PROX reaction, attaining high CO conversion and high selectivity towards CO_2 with low H_2 consumption at relatively low temperatures [19–27]. The excellent catalytic behaviour of the CuO-CeO_2 catalysts is attributed to their redox properties in the interface sites between CuO and CeO_2 particles. The well-known ability of CeO_2 to store and release oxygen [28] produces a promoting effect for ceria with fluorite-type structure, causing the partial modification of the oxidation state by the formation of a redox pair (Ce^{4+}-Ce^{3+}/Cu^{+}-Cu^{2+}). This leads to the formation of stabilised Cu^{+} species, which are the active species involved in the CO adsorption, while cerium oxide provides oxygen vacancies [29].

The redox parameters of the CuO-CeO_2 systems can be strongly influenced by the method of preparation of the catalysts, attaining different catalytic behaviour due to the different dispersion of the oxide species [21,30,31]. Several methods have been proposed in the literature to obtain efficient CuO-CeO_2 catalytic systems. Thus, an easy synthetic procedure to prepare a CuO-CeO_2 catalyst is by the combustion of nitrate precursors with urea [21]; however, this procedure can limit the number of CuO-CeO_2 interfaces, since the exothermic combustion of the urea can favour the sintering of both oxides. The precipitation of the catalytic precursors using a basic pH is another synthetic strategy [32]. The addition of a precipitating agent, usually in the form of NaOH or Na_2CO_3 solutions, can lead to the formation of heterogeneous particle size due to the formation of basic points when each drop of precipitating agent is added. A very slow co-precipitation followed by a long crystallisation step in the absence of organic additives leads to materials with peculiar architectures (shuttle-like, butterfly-like, or flower-like homocentric morphologies) where the higher degree of organisation can improve the catalytic activity [33]. An alternative to obtain more homogeneous particles is the use of urea, which decomposes into CO_2 and NH_3, causing an increase of the pH and the precipitation of the Cu and Ce species [34]. The thermal combustion of their respective precursors is another route to obtain CuO-CeO_2 systems [26,35]. The use of chelating agents, such as citric acid [25] or ethylenediaminetetraacetic acid (EDTA) [24], can improve the dispersion of the Cu and Ce species before calcination. In order to increase the porosity of the catalytic systems, several templates, such as poly(methyl methacrylate) (PMMA) microspheres [24] and polystyrene (PS) microspheres [36], or surfactants, such as hexadecyltrimethyl ammonium bromide [37] and Pluronic [38,39], have been used to increase the micro- and mesoporosity of the systems.

The aim of this research is to evaluate the influence of the preparation method on the redox behaviour of the CuO-CeO_2 catalysts. Thus, several CuO-CeO_2 catalysts were prepared by urea combustion, nitrate combustion, by complexing and calcination with citric acid and EDTA or by precipitation with NaOH and urea decomposition. The physicochemical properties of the prepared systems were correlated with the catalytic behaviour in the range 65–190 °C in the presence of an

H_2-rich feed. In addition, the catalytic resistance of the CuO-CeO_2 was evaluated for 48 h on stream. Finally, in order to simulate a CO-PROX unit cell, both CO_2 and H_2O streams were incorporated into the feed to evaluate the catalytic behaviour. Previous researches have evaluated the influence of H_2O and CO_2 on the stream; however, these studies only reported on CuO-CeO_2 systems synthesised by co-precipitation, urea-nitrate combustion or impregnation [40–47]. The catalytic behaviour of CuO-CeO_2 obtained from new synthetic strategies such as freeze-drying or using PMMA microspheres has not yet been compared with that of catalysts synthesised by traditional methods.

2. Results and Discussion

Several CuO-CeO_2 catalysts with the same Cu content (6 wt %) were synthesised by different synthetic methodologies: from the combustion of urea (U-Comb), from the calcination of their respective nitrates (N-Calc), by using NaOH as precipitating agent (Na-Prec), by precipitation from the thermal decomposition of urea (U-Prec), using poly(methyl methacrylate) microspheres (PMMA) as templates and by freeze-drying process (F-D).

Characterisation of the Catalysts

The diffraction peaks of the CuO-CeO_2 catalysts synthesised by different synthetic routes are shown in Figure 1. All profiles display diffraction peaks at 2θ (°) = 28.5, 33.2, 47.6, 56.2 and 59.1, which are assigned to the presence of the cubic fluorite structure of ceria (CeO_2) (PDF: 00-034-0394). Typical reflections of copper species are detected only in the case of the catalyst synthesised by the U-Comb route, where two small diffraction peaks are detected at 2θ (°) = 35.5 and 39.0, being ascribed to the presence of CuO species (PDF: 00-048-1548). This suggests a high dispersion degree of the CuO phase in the different catalytic systems.

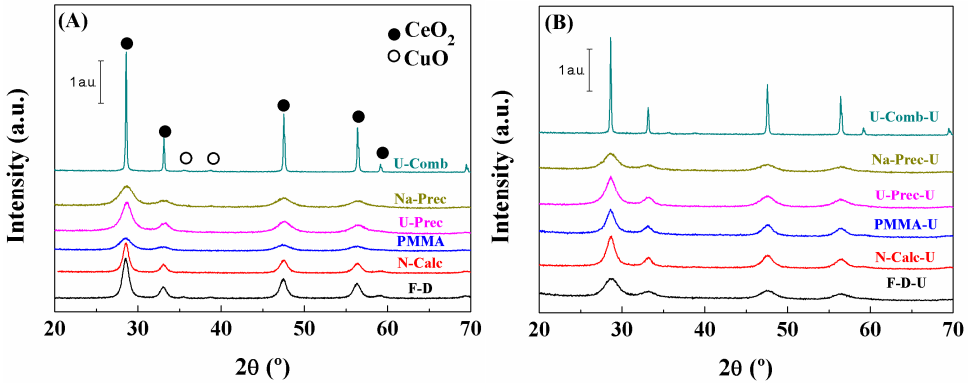

Figure 1. X-ray diffractograms of the CuO-CeO_2 catalysts obtained by several synthetic methods before the reaction (**A**) and after the reaction at 115 °C for 48 h of time on stream (TOS) (**B**).

The size of the CeO_2 particles was determined by the Williamson–Hall method [48] (Table 1). All catalysts displayed small CeO_2 crystals in the range 4–9 nm, except in the case of U-Comb catalyst, where the CeO_2 crystals were larger than 100 nm. This increase is in concordance with literature data and is due to the vigorous auto-ignition of the urea, which leads to sintering of the crystals [21,32]. Previous research has pointed out that the size and morphology of the ceria strongly affect the electronic structure in the CuO-CeO_2 interface, which is directly related to their catalytic behaviour [49,50]. On the other hand, the presence of smaller CeO_2 particles is associated to the existence of higher proportion of defects and imperfections on the border grain, which has a determining effect in the electronic transfer in the interfacial sites [50]. In the case of the U-Comb catalyst, the formation of well-defined CeO_2 crystals limits the formation of defects where takes place the oxygen storage/release so the modifications of the electronic interactions in the interfacial sites (Cu-O-Ce) for this catalyst should be limited.

The structural parameters of CeO_2, determined by the Rietveld method, show that all samples maintained the typical cell parameter of CeO_2 (a = 5.415 Å) [26], so the formation of $Ce_{1-x}Cu_xO_2$ solid solutions must be discarded.

Table 1. XRD characterisation and textural parameters of the CuO-CeO_2 catalysts.

Sample	Lattice Parameter (a/Å)	CeO_2 Particle Size (nm) [a]		Cu (wt %) [b]	Cu/Ce [b]	S_{BET} ($m^2 \cdot g^{-1}$)	t-Plot ($m^2 \cdot g^{-1}$)
		Fresh	Used				
F-D	5.412	9.9	4.9	6.1	0.06	18	7
N-Comb	5.411	6.7	7.3	7.1	0.06	85	49
PMMA	5.412	5.6	6.7	6.4	0.08	97	34
U-Prec	5.413	5.7	5.6	5.8	0.06	81	50
Na-Prec	5.421	4.7	4.6	7.2	0.07	135	74
U-Comb	5.410	101.0	91.7	5.5	0.06	7	1

[a] CeO_2 particle size determined by the Williamson-Hall equation for the fresh catalysts and the used catalysts after 48 h of TOS at 115 °C; [b] Data obtained by EDS analysis of TEM, using of average of 15 points.

The SEM images of the CuO-CeO_2 catalysts obtained from several synthetic methods are summarised in Figure 2. F-D catalyst (Figure 2A) displays a heterogeneous morphology with variable particle size from 1 to 200 μm. The PMMA catalyst (Figure 2B) also exhibits a heterogeneous morphology, although a more detailed study, using higher magnification, shows a honeycomb macroporous structure with a pore diameter about 300 nm. The catalysts synthesised by precipitation methods (Na-Prec and U-Prec) (Figure 2C,D) display the smallest particle size. Among them, U-Prec catalyst shows a larger particle size because the precipitation of Cu and Ce species take place more slowly, favouring the growth of the crystals. The N-Calc catalyst (Figure 2E) also displays heterogeneous crystals with a wide range of particle diameters. Finally, the U-Comb catalyst (Figure 2F) exhibits similar morphology to that observed in Figure 2E, although the exothermic process of the urea combustion generates pores of about 1 μm of diameter.

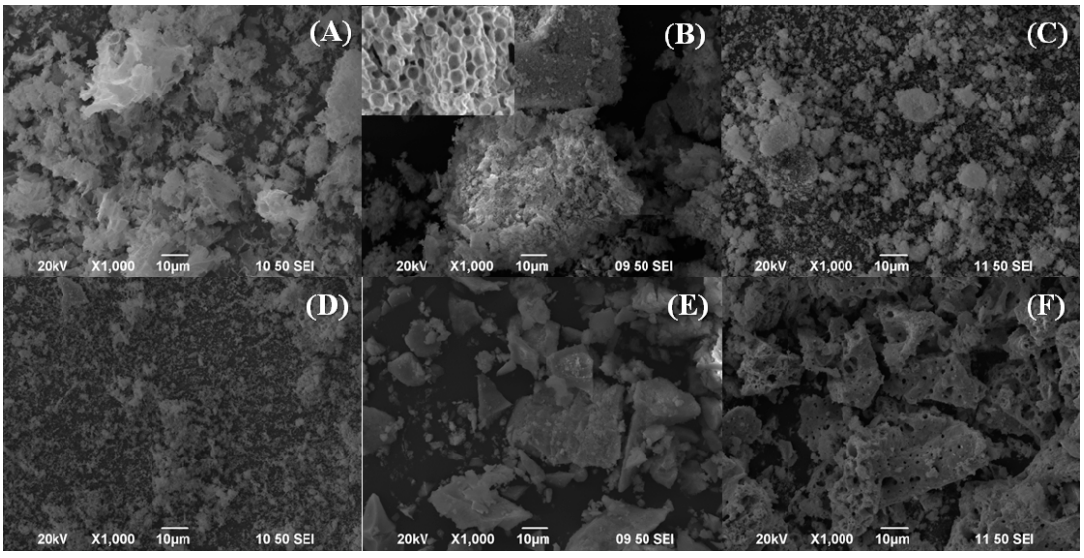

Figure 2. Scanning electron microscopy (SEM) images of the CuO-CeO_2 catalysts obtained by several synthetic methods (**A**) F-D, (**B**) PMMA, (**C**) Na-Prec, (**D**) U-Prec, (**E**) N-Calc and (**F**) U-Comb. (Magnification 1000×, scale 10 μm).

The TEM micrographs of the CuO-CeO_2 catalysts are summarised in Figure 3. The micrograph of the F-D catalyst (Figure 3A) shows heterogeneous particles with a variable size of several hundred nanometres, being formed by small CeO_2 and CuO particles which are agglomerated, as indicated by

energy disperse X-ray spectroscopy EDAX analysis (Supplementary Materials, Figure S1). In the case of the micrograph of the PMMA catalyst, Figure 3B shows the existence of a well-defined macroporous structure where small CuO-CeO_2 nanoparticles have been formed around the PMMA template. The micrograph of the Na-Prec catalyst (Figure 3C) exhibits a heterogeneous structure composed of small particles in the form of spheres and rods. A detailed study by EDAX (Supplementary Materials, Figure S1) indicates that the spherical structure is ascribed to CuO and CeO_2 particles, while the particles in form of rods are attributed to CeO_2 particles only. The TEM image of the U-Prec catalyst (Figure 3D) shows homogeneous spheres about 200 nm in size, which are composed of small CuO and CeO_2 nanoparticles. The image of the N-Calc catalyst (Figure 3E) reveals the existence of particles slightly larger than those shown in previous micrographs. However, these particles do not seem to exceed 10–15 nm. Finally, the micrograph of the U-Comb catalyst (Figure 3F) shows the largest particles due to the exothermic conditions of the synthesis, where it seems that the Cu particles are distributed over the CeO_2 crystals. The particle size obtained from the TEM micrographs of these six catalysts are comparable with data determined by the Williamson–Hall equation (Table 1).

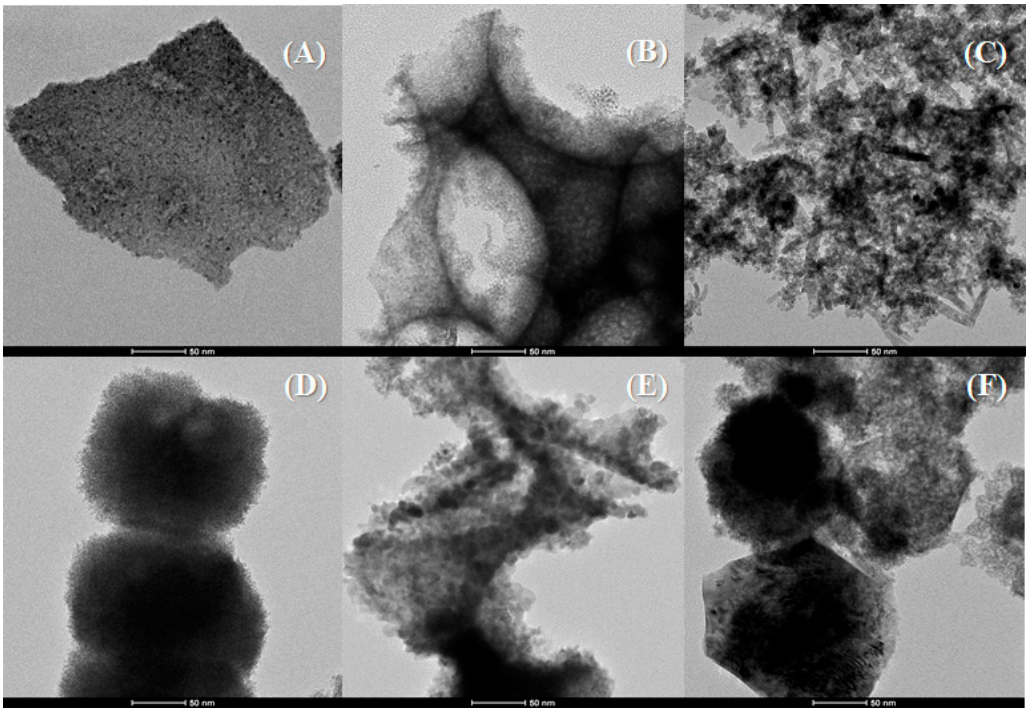

Figure 3. TEM images of the CuO-CeO_2 catalysts obtained by several synthetic methods (**A**) F-D, (**B**) PMMA, (**C**) Na-Prec, (**D**) U-Prec, (**E**) N-Calc and (**F**) U-Comb catalysts (scale 50 nm).

From EDX data, a semi-quantitative analysis was obtained considering an average of 15 points (Table 1). In all cases, the Cu charge is close to the theoretical loading (6 wt %), maintaining a similar Cu/Ce ratio for all the samples studied.

Raman spectra of the CuO-CeO_2 catalysts, compiled in Figure 4, provide information about the oxygen vacancies [51]. The Raman spectrum of the bulk CeO_2 displays a main peak located at 464 cm^{-1}, assigned to the F_{2g} vibrational mode of the cubic fluorite-type structure of CeO_2 [52]. All CuO-CeO_2 catalysts present the typical main peak of the CeO_2, although the maximum value is slightly shifted to lower frequency. Previous research has pointed out that the CeO_2 displays other vibration modes located at 585 and 250 cm^{-1} [32], which are attributed to the presence of oxygen vacancies. These bands are not identified in Figure 4, so the number of oxygen vacancies has to be relatively low. On the other hand, the typical bands of CuO species are not detected, confirming the high dispersion of the copper species, as indicated in the XRD data (Figure 1).

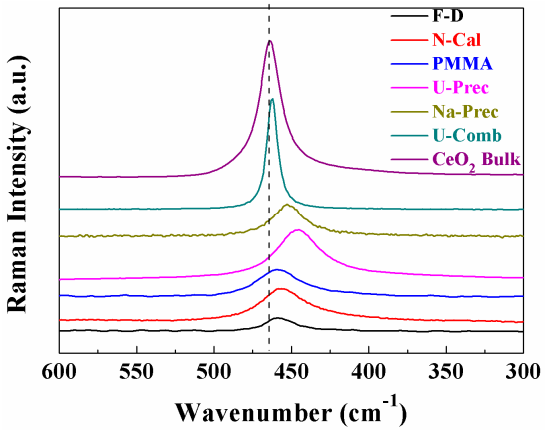

Figure 4. Raman spectra of the CuO-CeO_2 catalysts obtained by several synthetic methods (dashed line: F_{2g} vibrational mode of the bulk ceria).

Previous studies have pointed out that the shift of the F_{2g} vibrational mode can be assigned to the formation of solid solutions of CuO and CeO_2, which would cause modifications of the cell parameters; however the Rietveld data, shown in Table 1, reveals the same CeO_2 cell parameters in all CuO-CeO_2 catalysts [32,53]. Other authors have established a relationship between copper species and the shift of the F_{2g} vibrational mode, due to CuO particles that shield the CeO_2 framework [24,25]. From data shown in Figure 4, it can be concluded that the CuO-CeO_2 systems with smaller CeO_2 particles tend to suffer higher shielding than those with larger CeO_2 particles, such as the U-Comb catalyst, due to the their higher dispersion on the surface of the CeO_2.

The textural parameters of the CuO-CeO_2 catalysts were evaluated by N_2 adsorption–desorption at −196 °C (Figure 5). The N_2 isotherms reveal that all catalysts, except the Na-Prec catalyst, display a Type II isotherm, which is typical of non-porous or macroporous adsorbents. The porosity is attributed to the interparticle voids, or to the use of PMMA microspheres as templates that generate macropores after calcination. In the case of the Na-Prec catalyst, a Type IV isotherm can be observed with an H2 (b) hysteresis loop close to $P/P_0 = 1$, which is associated with pore blocking in a narrow range of pore necks or to cavitation-induced evaporation [54]. The specific surface area S_{BET}, obtained from the BET equation, reveals some differences between the systems studied (Table 1). Both F-D and U-Comb catalysts show the lowest S_{BET} values, while the samples synthesised by the precipitation method, N-Calc or by using PMMA exhibit higher S_{BET} values, reaching a maximum S_{BET} of 135 $m^2 \cdot g^{-1}$ for the Na-Prec catalyst. The reducibility of the CuO and CeO_2 species is a key parameter in the catalytic behaviour of the CO-PROX reaction. It is well known that CeO_2 reduction proceeds in two steps. The first reduction stage, between 300 and 650 °C, is assigned to the reduction of the unsaturated cerium species located on the surface, while the second reduction stage of CeO_2, at about 900 °C, is attributed to the reduction of bulk oxygen species [24]. The active oxygen species located at the interface between CuO and CeO_2 causes an enhancing of the reducibility of the catalytic system, leading to a reduction process at lower temperature [20].

H_2-TPR profiles of CuO-CeO_2 catalysts are compiled in Figure 6. Previous research established that the sequential reduction of copper ($Cu^{2+} \rightarrow Cu^{+} \rightarrow Cu^{0}$) is difficult to resolve in these experiments, so the different features observed in the samples have to be related to structural/morphological differences in the copper oxide entities involved [19]. Thus, all H_2-TPR profiles can be separated in several components. The first, denoted as (α) and located at lower temperature, is attributed to the reduction of highly dispersed copper oxide species, strongly interacting with ceria, which includes isolated copper ions and small two- and three-dimensional clusters. The peak denoted as (β) is attributed to well-dispersed larger CuO cluster species weakly interacting with CeO_2. The peak located at higher temperature (γ) is assigned to larger CuO bulk-like particles associated with the ceria [22,55]. An H_2-TPR profile with a higher H_2 consumption ascribed to α and β peaks confirms

the presence of well-dispersed copper oxide species in the catalytic system. This is the trend for all the samples, except for the U-Comb catalyst, where the H_2 profile is shifted to higher temperature, probably due to the presence of larger copper oxide agglomerates as a consequence of the CuO sintering by the exothermic character of the urea combustion, as was suggested by XRD data (Figure 1).

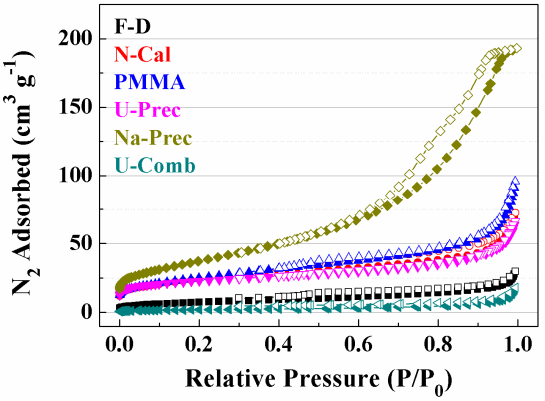

Figure 5. N_2 adsorption–desorption isotherms of CuO-CeO_2 catalysts obtained by several synthetic methods (solid symbol: adsorption branch and open symbol: desorption branch).

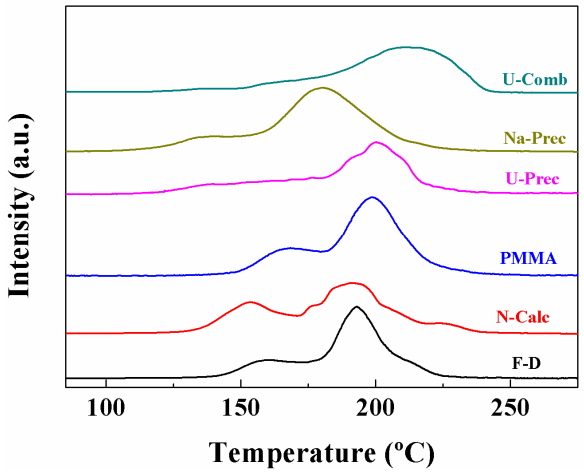

Figure 6. H_2-TPR profiles of the CuO-CeO_2 catalysts obtained by several synthetic methods.

The theoretical H_2 consumption of the CuO-CeO_2 with a copper loading of 6 wt % is 944 μmol·g^{-1}. This value was obtained considering the theoretical amount of CuO set in each H_2-TPR. The H_2 quantification from TPR profiles reveals that H_2 consumption of all catalysts is higher than theoretical (Table 2), indicating the simultaneous reduction of CuO species and the surface of the CeO_2 [24,26,27,32]. In fact, a relationship can be established between the CeO_2 particle size and its H_2-consumed/H_2-theoretical ratio. Thus, the catalysts with lower CeO_2 particle size, such as those obtained by precipitation methods, must possess a larger proportion of unsaturated ceria more easily reducible than those catalysts with bigger crystals, such as the U-Comb catalyst, where external ceria surface area must be lower due to its largest particle size and lowest BET surface area. This leads to the reduction of CuO and unsaturated cerium species located on the surface overlapping, as indicated by the H_2-consumed/H_2-theoretical ratio being greater than unity. This value is higher for catalysts with smaller CeO_2 crystal size, due to the presence of a higher proportion of reducible superficial cerium species. In this sense, previous research have pointed out that the catalysts with smaller CeO_2 size exhibit higher modifications in the Cu sites in comparison to bare CuO by a transfer of small amount of electron for copper to ceria [56] due to the perturbations in their electronic properties due

to the ability to store/release oxygen species of CeO_2. In the case of the U-Comb catalyst, the bigger CuO crystals act similarly to the CuO bulk, which diminishes the electronic modifications, leading to a CuO/CeO_2 catalyst with lower reducibility of both Cu^{2+} and Ce^{4+} species, which supposes a catalyst with lower potential for the CO-PROX reaction [57,58]. In the same way, Liu et al. have pointed out that the incorporation of CuO particles on the surface of CeO_2 acts as a seed for the formation of higher proportion of oxygen vacancies [59]. The samples with higher dispersion and lower particle size favours this synergistic effect by an electronic transfer between Cu^{2+} species and CeO_2, increasing the reducibility of the catalytic system, which is a key factor for the CO-PROX activity.

Table 2. Reducibility degree obtained from H_2-TPR profiles for $CuO\text{-}CeO_2$ catalysts synthesised by several synthetic methods.

Sample	α Peak (%)	β Peak (%)	γ Peak (%)	T_{MAX} (°C)	H_2 Consumption ($\mu mol \cdot g^{-1}$)	H_2 Consumed/H_2 Theoretical
F-D	24.6	59.3	16.1	193	1088	1.20
N-Calc	30.0	64.0	6	192	1184	1.26
PMMA	35.8	64.2	-	176	1162	1.23
U-Prec	16.8	83.2	-	202	1284	1.36
Na-Prec	26.7	56.2	17.1	180	1312	1.39
U-Comb	2.8	10.4	86.8	215	972	1.03

The surface composition of the materials was evaluated by XPS (Figure 7 and Table 3). All experiments were carried out with short exposition times of about 8 min, to avoid the photoreduction of both Ce and Cu species.

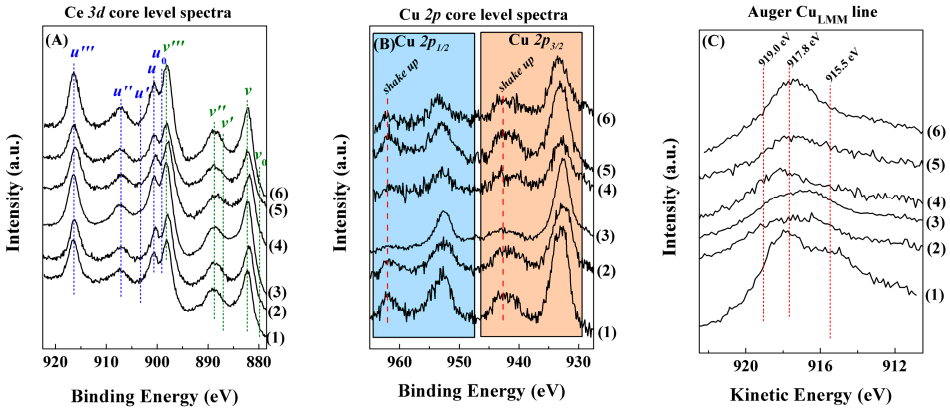

Figure 7. Ce 3*d* core level spectra (**A**), Cu 2*p* core level spectra (**B**) and Auger Cu_{LMM} line (**C**) of $CuO\text{-}CeO_2$ catalysts obtained by several synthetic methods: (1) F-D, (2) N-Calc, (3) PMMA, (4) U-Prec, (5) Na-Prec and (6) U-Comb catalysts.

Table 3. Spectral parameters of $CuO\text{-}CeO_2$ catalysts synthesised by different methodologies [a].

Sample	I_{Sat}/I_{mp}	Ce^{3+}/Ce^{4+}	Cu/Ce	Cu_{LMM} (eV)
F-D	0.36 (0.31)	0.32 (0.40)	0.27 (0.47)	917.8 (917.9)
N-Calc	0.29 (0.24)	0.08 (0.03)	0.45 (0.67)	917.4 (916.8)
PMMA	0.45 (0.37)	0.10 (0.18)	0.35 (0.37)	916.7 (916.0)
U-Prec	0.40 (0.33)	0.12 (0.07)	0.28 (0.36)	918.1 (918.2)
Na-Prec	0.38 (0.34)	0.11 (0.09)	0.19 (0.22)	917.2 (918.0)
U-Comb	0.42 (0.35)	0.06 (0.07)	0.48 (0.55)	918.1 (917.5)

[a] In brackets, the spectral parameters of $CuO\text{-}CeO_2$ used catalysts after 48 h of TOS at 115 °C.

The Ce 3*d* core level spectra (Figure 7A) are composed of 10 contributions: *v*, *u* (Ce $3d^9\ 4f^2\ O\ 2p^4$) and *v*″, *u*″ (Ce $3d^9\ 4f^1\ O\ 2p^5$); *v*‴, *u*‴ (final state of Ce $3d^9\ 4f^0\ O\ 2p^6$) assigned to Ce^{4+} species and v^0,

u^0 (Ce $3d^9$ $4f^2$ O $2p^5$) and v', u' (Ce $3d^9$ $4f^1$ O $2p^6$) assigned to Ce^{3+} species as a consequence of the hybridisation between the Ce 4*f* levels and the O 2*p* states [60]. In all cases, the main contributions have been ascribed to the presence of Ce^{4+} species, although Ce^{3+} species have been also detected, as the Ce^{3+}/Ce^{4+} ratio indicates (Table 3). These data can be related to the H_2-consumed/H_2-theoretical ratio (Table 2) due to the formation of smaller particles that lead to a higher proportion of surface area, which is more easily reducible [61]. However, these data are not in accordance with the Raman spectra, so it is expected that Ce species tend to undergo a photoreduction process despite the short irradiation time.

The Cu 2*p* core level spectra of the CuO-CeO_2 catalysts are shown in Figure 7B. The Cu $2p_{3/2}$ region contains two bands. The first, located between 932.5–933.0 eV, is attributed to the overlapping of a contribution assigned to reduced copper species ($Cu^{0/+}$), which appears at about 932.5 eV and another contribution attributed to Cu^{2+} species, at about 935.5 eV [60]. The second band, with a maximum at 942.4 eV, is attributed to the existence of a shake-up satellite, which is typical of divalent species [60]. The analysis of the ratio between the area of the main peak and the area of all peaks including the satellite (I_{sat}/I_{mp}) allows the determination of the reduced copper species. Previous research has pointed out that pure CuO displays an I_{sat}/I_{mp} ratio of 0.55 [21]. The spectral parameters shown in Table 3 reveal that all CuO-CeO_2 catalysts display similar I_{sat}/I_{mp} values (0.29–0.45), which are lower than the theoretical data, confirming the coexistence of Cu^{2+} and reduced Cu species.

In order to discern between reduced Cu species, i.e., Cu^0 and Cu^+, the Cu_{LMM} Auger line was also studied (Figure 7C). In all cases, the main band is located at 917 eV, indicating the presence of Cu^{2+} species. In addition, it is noticeable the presence of a shoulder at 915 eV, which confirms the presence of Cu^+. In this sense, Cu^+ species are the ones involved in the adsorption of CO in the CO-PROX reaction [40,44]. Finally, the absence of a band at 919 eV discards the presence of Cu^0 species [26].

Considering the atomic concentration determined by EDAX (Table 1), it can be observed that all catalysts display ratios above the EDAX data, suggesting that there is a higher proportion of Cu species located on the surface of the catalysts. Generally, it can be observed that the CuO-CeO_2 catalysts synthesised with a calcination step in the procedure, such as PMMA or U-Comb catalysts, show higher Cu/Ce ratio than those synthesised under milder conditions, such as by the co-precipitation method. In the case of the F-D catalyst, the Cu/Ce ratio is close to that obtained for CuO-CeO_2 synthesised by precipitation, which can be ascribed to the milder calcination conditions in comparison to the other synthetic procedures. This observation is more pronounced in the case of the U-Comb catalyst, where the exothermic process affects to the dispersion of the active phase, provoking an increase in the Cu content on the surface of the catalyst. The higher amount of Cu on the surface of the catalytic system should indicate a high number of available sites; however, its high crystallinity, lower porosity and reducibility limit its catalytic behaviour in the CO-PROX reaction.

The O 1*s* core level spectra show an asymmetric band, which can be separated into two components located at 529.2 eV, ascribed to oxide species, and another contribution at 531.3 eV, attributed to the presence of hydroxyl or carbonate species [24,25,62].

With regard to the C 1*s*, together with the adventitious carbon located at 284.8 eV, the presence of a smaller contribution located at 288.8 eV is noteworthy, assigned to the presence of carbonate species resulting from the re-carbonation of the CuO-CeO_2 catalysts [24,25].

3. Catalytic Results

The catalytic behaviour of the CuO-CeO_2 samples synthesised by different methods was evaluated in the CO-PROX reaction between 65 and 190 °C (Figure 8). In all cases, the only reactions that proceeded were the CO and H_2 oxidations, while both methanation and reverse water gas shift reaction were negligible under the catalytic conditions used in this study.

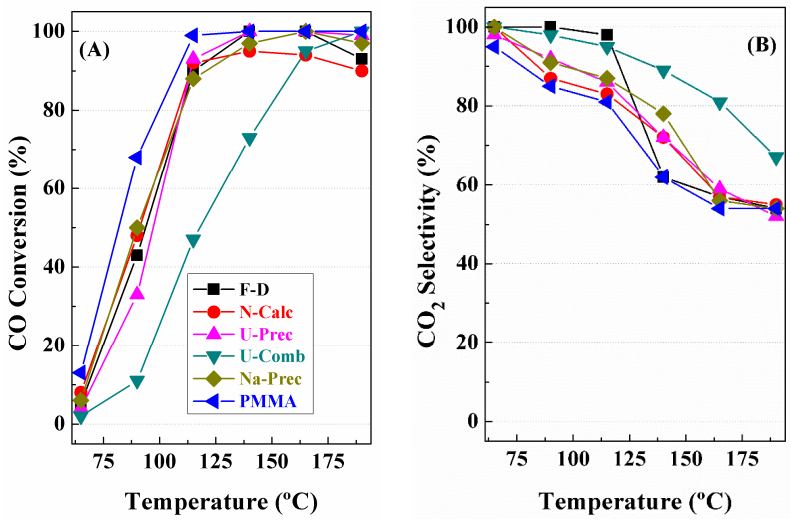

Figure 8. CO conversion (**A**) and selectivity toward CO_2 (**B**) as function of the temperature of CuO-CeO_2 catalysts. Operating conditions: Gas hourly space velocity (GHSV) = 22,000 h^{-1}, λ = 2, 1.25% CO, 1.25% O_2, 50% H_2, He balance (vol %).

From catalytic data shown in Figure 8A, it can be observed how the CO conversion increases with the reaction temperature attaining a conversion value close to 100% at 115 °C with the PMMA catalyst. The remaining catalysts reached a CO conversion of between 90% and 95% at 115 °C, except the U-Comb catalyst, which reached a CO conversion of only 48% at 115 °C. Nonetheless, the use of higher reaction temperatures gave rise to a catalytic conversion in the range 90–100% in all cases.

The excellent performance of most CuO-CeO_2 catalysts is attributed to the small particle size of ceria (5–9 nm), which favours the formation of high proportion of interfacial sites where preferential CO oxidation takes places [20,22]. The similar CeO_2 crystal size leads to similar catalytic behaviour. In this sense, the Cu/Ce molar ratio on the surface of the catalysts (Table 3) has established that the catalysts synthesised from combustion processes (N-Calc and U-Comb) have higher Cu/Ce ratios, which suggests higher dispersion of the CuO species on the CeO_2, resulting in conversion values. However, the N-Calc catalyst exhibited higher conversion values at lower temperature compared to the U-Comb catalyst. This can be ascribed to the bigger CeO_2 crystal size together with its lower specific surface area (7 $m^2 \cdot g^{-1}$), which implies a lower number of active sites available for the CO-PROX reaction [20], limiting the CO conversion. In this sense, it is well known that reducibility of CuO-CeO_2 is closely related to the formation of partially reduced copper species, which are necessary for the CO-PROX reaction [19,20,22,44]. Thus, the U-Comb catalyst, with a lower reducibility, showed the lowest conversion values between 95 and 165 °C. In all cases, an increase of the temperature causes a gradual transformation of Cu^{2+} to Cu^{+} and Cu^{0}. The electronic interactions between Cu and ceria facilitates the reducibility of the Cu species by the redox equilibrium ($Cu^{4+} + Cu^{+} \leftrightarrow Ce^{3+} + Cu^{2+}$) in comparison to bare CuO so Cu^{2+} is the predominant specie at low temperature, while a progressive increase of the reaction temperature leads to Cu^{+} and Cu^{0} species. The use of temperature in the range 95–165 °C leads to a partial reduction of the Cu^{2+} to Cu^{+} species, which are the active species in the CO-PROX reaction by the formation of Cu^{+}-carbonyl species and subsequent oxidation to CO_2 [63]. In the case of the U-Comb catalyst, the lower reducibility of the CuO-CeO_2 catalyst diminishes in the presence of bigger CeO_2 crystals, which limits the oxygen mobility. This implies that Cu^{2+} is the main copper specie in this range of temperature, leading to poorer catalytic activity in comparison to the other catalysts.

With regard to selectivity (Figure 8B), all CuO-CeO_2 catalysts displayed a selectivity towards CO_2 of 100% at low temperature (65 °C) due to the excess oxygen added in the feed favouring the oxidation of CO to CO_2 at low temperature. The increase in reaction temperature caused a decrease in

CO_2 selectivity due to the competitive oxidation reaction that occurs in the same range of temperature for both CO and H_2 species by the partially reduced Cu active sites [20,27]. It has been reported that the use of lower temperature favours the presence of Cu^{2+} and Cu^{+} species, which are involved in the CO oxidation reaction; however, an increase in the reaction temperature leads to the formation of reduced copper species (Cu^0), causing the oxidation of H_2 species [63]. The selectivity pattern can be related to the particle size of the CeO_2 since the presence of smaller CeO_2 crystals enhances the mobility of oxygen species, increasing the reducibility of the CuO-CeO_2 system. In the case of the U-Comb catalyst, which presents a lower proportion of available partially reduced copper species due to the existence of bigger CeO_2 crystals, it displays a lower CO conversion and higher CO_2 selectivity at low temperature in comparison with the other CuO-CeO_2 systems.

In summary, the data obtained in Figure 8 show an almost full CO conversion from 115 °C for all CuO-CeO_2 samples, except U-Comb catalyst. The catalysts used in large-scale, i.e., Pt- and Ru-based catalysts, require a lower reaction temperature to obtain full conversion (40–60 °C) with high selectivity to CO_2 [12]. Nonetheless, the high cost of these noble metals has led to the development of inexpensive alternative such as CuO-CeO_2 catalysts, which need a higher reaction temperature to obtain adequate conversion values, although within the range of the PEMFC fuels.

Catalytic stability is a key factor in obtaining competitive catalysts. For this purpose, all CuO-CeO_2 catalysts were assayed within the working temperature range of PEMFC cells (115 °C). The catalytic data, compiled in Figure 9, show how all CuO-CeO_2 catalysts hardly suffer any deactivation during 48 h time on stream (TOS), reaching CO conversions close to 90–100% with CO_2 selectivity of 80–90% for most catalysts, leading to highly competitive catalytic systems in the H_2 purification processes.

In order to evaluate possible modifications of the active phase along the catalytic process, the catalysts were recovered after the stability tests and kept in an inert solvent, such as cyclohexane, to be characterised by XRD and XPS.

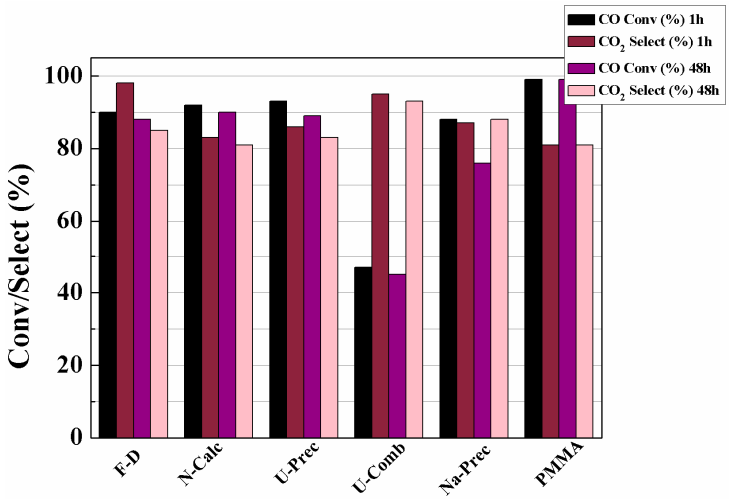

Figure 9. CO conversion and selectivity toward CO_2 after 1 h and 48 h of TOS of CuO-CeO_2 catalysts. Operating conditions: T_{reac} = 115 °C, Gas hourly space velocity (GHSV) = 22,000 h^{-1}, λ = 2, 1.25% CO, 1.25% O_2, 50% H_2, He balance (vol %).

The X-ray diffractograms of the catalysts used (Figure 1B) reveal how the typical diffraction peaks of CeO_2 were maintained after the catalytic tests. In addition, diffraction peaks attributed to copper species were not detected in the XRD profiles of the materials, suggesting that these species maintain a high dispersion after the 48-h stability test. The estimation of the CeO_2 particle size by the Williamson–Hall equation [48] (Table 1) shows how the CeO_2 maintains its particle size after the stability test. In summary, the XRD data of the used catalysts discard the modification of CeO_2 to another Ce-species and the sintering of both CeO_2 and Cu species.

With regard to the XPS spectra (Figure 10), Ce 3*d* core level spectra of the used catalysts (Figure 10A) display similar profiles and Ce^{3+}/Ce^{4+} ratio than their respective spectra before the catalytic tests. In all cases, the Ce^{3+}/Ce^{4+} molar ratios are maintained, confirming the chemical stability of CeO_2, as previously indicated in the XRD data (Figure 1).

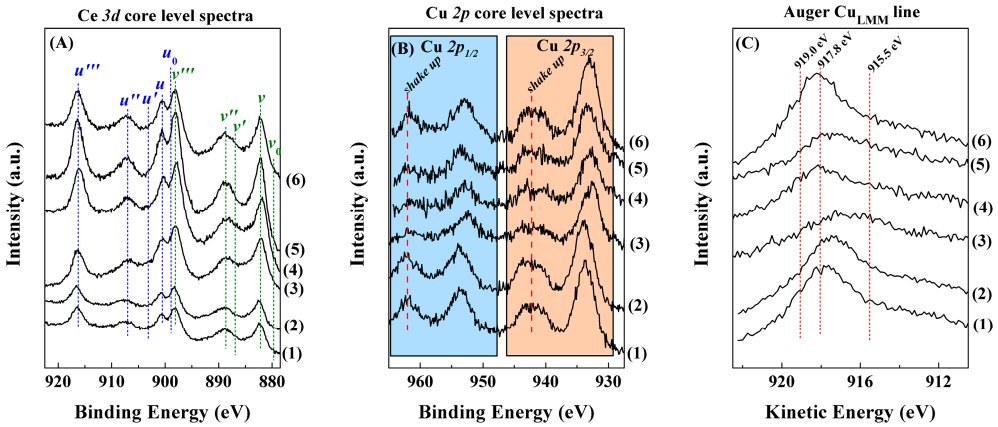

Figure 10. Ce 3*d* core level spectra (**A**), Cu 2*p* core level spectra (**B**) and Auger Cu_{LMM} line (**C**) of the used CuO-CeO_2 catalysts (after 48 h of TOS at 115 °C) obtained by several synthetic methods: (1) F-D, (2) N-Calc, (3) PMMA, (4) U-Prec, (5) Na-Prec and (6) U-Comb catalysts.

The Cu 2*p* core level spectra (Figure 10B) also exhibit similar bands to before the reaction, i.e., a band at 933.0 eV attributed to Cu species and another at 942.5 eV ascribed to the shake-up satellite. Analysis of the I_{sat}/I_{mp} ratio after the stability test (Table 3) shows a slight decrease in their values in comparison to the catalyst before the CO-PROX reaction, which suggests the partial reduction of the copper species due to the use of H_2-rich feed after 48 h TOS at 115 °C, in accordance with the H_2-TPR profile (Figure 5). The Auger Cu_{LMM} line (Figure 10C) shows a slight increase of the Cu^+ signal, which indicates the formation of catalytically active species during the CO-PROX reaction. Finally, in spite of H_2-rich feed, the presence of Cu^0 species cannot be observed in any case, so the redox pair ratio ($Ce^{4+/3+}/Cu^{+/2+}$) is maintained after 48 h TOS. In any case, the similarity between the XPS profile before and after the catalytic reaction reflects the high stability of all CuO-CeO_2 catalysts after 48 h.

With regard to the Cu/Ce atomic ratio, an increase of the Cu content on the surface can be observed for all CuO-CeO_2 catalysts (Table 3), which indicates a slight decrease in the dispersion of the Cu particles and therefore a decrease in the number of available interfacial sites.

Finally, in order to simulate the real conditions of H_2 purification, 15 vol % CO_2 and 10 vol % H_2O were added to the feed to establish similar conditions to those produced by the water gas shift reaction in the range 115–190 °C (Figure 11).

It has been reported in the literature that the presence of CO_2 and H_2O in the feed has an inhibitive effect in the CO-PROX reaction. The presence of CO_2 in the feed leads to a competitive effect between CO and CO_2 on the Cu^+ sites [47]. In addition, the strong Cu^+-CO_2 interaction requires high temperatures to favour the desorption of the CO_2 molecules and thus make available the active centres for the CO-PROX reaction [64]. The presence of H_2O in the feed has a stronger inhibitive effect in this reaction due to blockage of the active centres [21]. The results of the catalytic experiments in the presence of CO_2 and H_2O follow a different trend from those shown in the elementary tests. This suggests that other parameters, such as the textural properties, are involved in the catalytic behaviour. Thus, all the catalysts, except PMMA (Table 1), shift their CO conversion at higher temperatures. The excellent catalytic behaviour of the PMMA catalyst can be attributed not only to the small CeO_2 particle size and the larger amount of easily reducible copper oxide species, strongly interacting with ceria, but also to the peculiar morphology and porosity of the material (Table 2, Figures 2 and 3), since the existence of macropores can minimise the blockage of the active sites by

H_2O. It is furthermore noticeable that a CO conversion close to 95% is obtained at 115 °C, simulating the real conditions of a PROX unit at the working temperature of a PEM fuel cell. These data are higher than those reported in the literature for catalysts produced by traditional synthetic strategies, such as impregnation or precipitation, where high conversion values are between 170 and 200 °C [42,43,46].

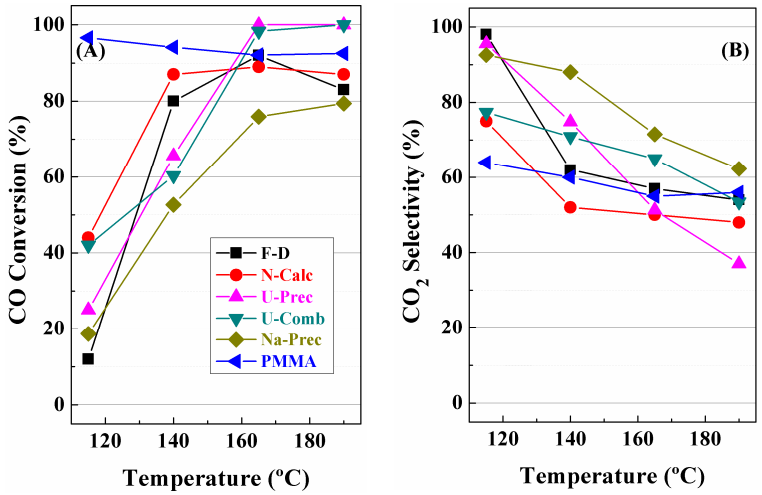

Figure 11. CO conversion (**A**) and selectivity toward CO_2 (**B**) as a function of the temperature of CuO-CeO_2 catalysts. Operating conditions: Gas hourly space velocity (GHSV) = 22,000 h^{-1}, λ = 2, 1.25% CO, 1.25% O_2, 50% H_2, 10% H_2O, 15% CO_2, He balance (vol %).

Considering the CO behaviour of the CuO-CeO_2 catalysts in the CO-PROX reaction, future studies must be focused on the comparison of the CO conversion and CO_2 selectivity with the noble metal-based catalysts. In addition, CuO-CeO_2-based catalysts should be evaluated in monoliths to simulate the conditions at a larger scale. Moreover, the stability of these catalysts must be evaluated by testing several runs of each catalyst.

4. Materials and Methods

4.1. Catalyst Preparation

4.1.1. CeO_2-CuO from Calcination of Nitrate Precursors (N-Calc)

CeO_2-CuO catalyst was synthesised following the procedure described by Cecilia et al. [26]. Briefly, the precursor $Ce(NO_3)_3{\cdot}6H_2O$ (99.99%, Aldrich, St. Louis, MO, USA) was calcined to 500 °C at a rate of 10 °C·min^{-1}, maintaining this temperature for 2 h. The copper-containing catalyst was prepared by incipient wetness impregnation of the supports with a solution of copper(II) nitrate (99.99%, Aldrich) and the solid dried overnight at 60 °C and calcined for 4 h at 400 °C.

4.1.2. CeO_2-CuO from Thermal Urea-Nitrate Combustion (U-Comb)

CeO_2-CuO catalyst obtained by thermal urea-nitrate combustion was synthesised according to the procedure of Avgouropoulos and Ioannides [21]. Both $Ce(NO_3)_3{\cdot}6H_2O$ and $Cu(NO_3)_2{\cdot}6H_2O$ were dissolved in the minimum volume of distilled water, then urea added using a urea/nitrate molar ratio of 2.5:1. The solution was heated for a few minutes at 80 °C and then the gel was placed into an oven, preheated to 400 °C, resulting in a foamy structure by the spontaneous combustion of urea. Finally, the solid was recalcined at 400 °C for 2 h to remove the carbonaceous deposits.

4.1.3. CeO_2-CuO from Freeze-Drying (F-D)

According to the method of Arango-Díaz et al. [24], both $Ce(NO_3)_3 \cdot 6H_2O$ and $Cu(NO_3)_2 \cdot 6H_2O$ were dissolved in water. Later ethylenediaminetetraacetic acid (EDTA 99.7%, Aldrich) was added as complexing agent to prevent precipitation in a 1:1 ligand/metal molar ratio, adjusting the pH to 7–8 by adding aqueous ammonia. The solution was flash frozen dropwise into liquid N_2 and dried in a freeze-dryer for three days. The precursor obtained was calcined at 300 °C for 2 h to remove the organic matter and avoid rehydration.

4.1.4. CeO_2-CuO Using Poly(methyl metacrylate) (PMMA) as a Template

PMMA spheres of about 400 nm were synthesised from emulsion polymerisation of methyl methacrylate (MMA) in aqueous solution, using 2,2′-azobis(2-methylpropionamidine) dihydrochloride (97%, Aldrich) as a radical initiator [65]. $Ce(NO_3)_3 \cdot 6H_2O$ and $Cu(NO_3)_2 \cdot 6H_2O$ were dissolved by stirring in an aqueous solution of pH = 3. PMMA spheres were added to the solution with a PMMA/catalyst mass ratio of 3.5:1, maintaining the stirring for 15 min. The solvent was slowly evaporated in ambient conditions for three days, the solid dried at 60 °C for 1 h and calcined at 400 °C for 4 h to remove the template spheres, leading to a regular porous structure [25].

4.1.5. CeO_2-CuO from Precipitation Method Using NaOH as a Precipitating Agent (Na-Prec)

CeO_2-CuO was synthesised by the co-precipitating method using aqueous $Ce(NO_3)_3 \cdot 6H_2O$ and $Cu(NO_3)_2 \cdot 6H_2O$ solutions at a concentration of 0.3 M. Aqueous NaOH 0.3 M was added slowly to the mother liquor until a pH of 11 was reached, leading to the precipitation of both copper and cerium hydroxides. The obtained precipitate was aged for 4 h at 60 °C, and then at room temperature for 12 h. The solid was filtered and washed with deionised water to neutral pH to ensure the removal of Na^+ species. Finally, the solid was dried for 12 h at room temperature and calcined at 400 °C, maintaining this temperature for 4 h [66].

4.1.6. CeO_2-CuO Synthesised from the Combustion of Urea as a Precipitating Agent (U-Prec)

CeO_2-CuO were co-precipitated from 0.3 M solutions of $Ce(NO_3)_3 \cdot 6H_2O$ and $Cu(NO_3)_2 \cdot 6H_2O$. Urea was added dropwise using a urea/nitrate molar ratio of 4:1 and the solution stirred and heated at 90 °C to decompose urea to CO_2 and NH_3. In order to ensure total precipitation, the obtained solid was stirred at 90 °C for 24 h and then this solid was filtered and washed with water. Finally, the solid was dried for 12 h and calcined at 400 °C for 4 h, at a heating rate of 1 °C·min^{-1} [34].

In all cases, CNH analyses were carried out to ensure the removal of nitrogen and carbon species after the calcination step, obtaining a nitrogen or carbon content lower than 0.5 wt % in all cases.

All samples were synthesised with a nominal copper loading of 6 wt %, considering that several authors have pointed that the maximum CO conversion in the CO-PROX is obtained at a Cu content of 6–7 wt % [22,62].

4.2. Characterisation of the Catalysts

Powder patterns for the samples were analysed on a X'Pert Pro MPD automated diffractometer (PANalytical B.V., Almelo, The Netherlands), which is equipped with a Ge(111) primary monochromator with monochromatic Cu Kα_1 radiation and a X'Celerator detector with a step size of 0.017°. The powder patterns were measured between 10° and 70° in 2θ. The particle size of the catalysts was determined by the Williamson–Hall method from fitting of the diffraction profile [48]. The cell parameters were estimated from the Rietveld method.

The microstructure and morphology of the CuO-CeO_2 catalysts was determined using Scanning Electron Microscopy (SEM). The catalysts were gold-coated in a JEOL Ion Sputter JFC-1100 device (gold coat w300 Å thick, Akishima, Tokyo, Japan). Then, they were observed in a JEOL JSM-6490LV scanning electron microscope (Akishima) using secondary electrons.

The morphology of the catalysts was studied by Transmission Electron Microscopy (TEM), using FEI Talos F200X equipment (Thermo Fisher Scientific, Waltham, MA, USA) that combined outstanding high-resolution S/TEM and TEM imaging with industry-leading energy dispersive X-ray spectroscopy (EDS) signal detection, and 3D chemical characterisation with compositional mapping. The samples were suspended in isopropyl alcohol and dropped onto a perforated carbon film grid.

The Raman spectra were carried out using a BRUKER RAM II Raman spectrometer (Bruker, Billerica, MA, USA) with a Ge detector using an excitation line of 1064 nm with Nd-YAG laser. The data were measured maintaining the power at 30 mW, a standard spectral resolution of 4 cm^{-1} and 2000 accumulations for each spectrum. Operation was at liquid N_2 temperature. In order to carry out the analysis, the samples were pressed into small discs and then placed on the analytic chamber. The Raman scattering measurements were carried out in the 200–800 cm^{-1} region.

The textural parameters of the CuO-CeO_2 catalysts were estimated from the N_2 adsorption–desorption isotherms at −196 °C using an automatic ASAP 2020 system supplied from Micromeritics (Norcross, GA, USA). Prior to the N_2 adsorption–desorption, samples were degassed at 200 °C and 10^{-4} mbar overnight. Surface areas were estimated by using the Brunauer–Emmett–Teller (BET) method [67].

H_2 thermoprogrammed reduction (H_2-TPR) analysis were carried out on 0.080 g of catalyst immediately after calcination at 400 °C to remove the possible products of recarbonation of cerium and copper oxide species. Each sample was cleaned with a He flow (35 mL min^{-1}) at 100 °C for 30 min and then cooled to 40 °C. The H_2 consumption was measured between 100 and 800 °C, using an Ar/H_2 flow (48 mL·min^{-1}, 10 vol % H_2) and at a heating ramp of 10 °C·min^{-1}. Water formed in the reduction reaction was retained using an isopropanol–liquid nitrogen as trap and a cold finger (−80 °C). The H_2 consumption was measured with a thermal conductivity detector (TCD). The H_2 consumed thermoprogrammed reduction experiments was determined by calibration with pure CuO (Aldrich) as reference, assuming that all CuO is reduced to Cu^0.

X-ray photoelectron spectra were carried out using a Physical Electronics PHI 5700 spectrometer (Ulvac-Phi, Chanhassen, MN, USA), which is equipped with non-monochromatic Mg Kα radiation (300 W, 15 kV and 1253.6 eV) and a multichannel detector. All spectra were measured using a constant pass energy mode at 29.35 eV, using a diameter analysis area of 720 μm. In all cases, the adventitious carbon (C 1*s* at 284.8 eV) was used as reference. A PHI ACCESS ESCA-V6.0F software package (Ulvac-Phi) was used for acquisition and data analysis. The signals were substrated considering a Shirley-type background and were fitted using Gaussian–Lorentzian curves to estimate the binding energies of the different element core levels. In order to avoid the photoreduction of Ce^{4+} and Cu^{2+} species as much as possible, short irradiation time spectra of Ce 3*d*, Cu 2*p* and C 1*s* were first registered. Nevertheless, the reduction of Ce^{4+} and Cu^{2+} in high vacuum conditions could not be excluded. The Auger parameter was determined from the following equation:

$$\alpha_0 = KE_{\mathrm{CuLMM}} - 1253.6 \quad (1)$$

4.3. Catalytic Tests

Catalytic experiments were carried out using a fixed-bed reactor at atmospheric pressure. All catalysts were performed with an amount of catalyst of 0.150 g, which was sieved (0.050–0.110 mm) previously. The catalyst was putted in a tubular stainless steel reactor with an internal diameter of 5 mm and a thermocouple in direct contact with the catalyst. Prior the test, the catalyst was pretreated in situ under N_2/O_2 (80:20 vol %) flow (30 mL·min^{-1}) for 30 min at 400 °C. Then, the catalyst was cooled to 65 °C in He flow. The experiments were carried out with a (W/F) of 0.18 g·s·cm^{-3} (GHSV = 22,000 h^{-1}). The reaction mixture composition was 1.25% CO, 1.25% O_2, 50% H_2, balanced with He for the elementary tests. The overall CO-PROX reaction is:

$$CO + ½\, O_2 \rightarrow CO_2 \quad (2)$$

$$H_2 + ½\, O_2 \rightarrow H_2O. \quad (3)$$

The effect of CO_2 and H_2O was examined with the addition of 15% CO_2 and 10% H_2O. An ice-salt cooled cold finger (−20 °C) was used to trap the water downstream from the reactor. A Shimadzu-GC-2014 gas chromatograph (Shimadzu, Kyoto, Japan) equipped with TCD and a Carboxen 1000 60/80 mesh column was used to analyse the outlet composition. The reaction temperature was varied from 65 to 190 °C, maintaining the reaction for 1 h at each temperature. Several measurements were carried out until a steady state was achieved for each experimental point.

The CO (Equation (4)) and O_2 (Equation (5)) conversions (X_{CO} and X_{O_2}, respectively) were calculated based on the CO and O_2 consumption, respectively:

$$X_{CO}\ (\%) = \frac{n_{CO}^{in} - n_{CO}^{out}}{n_{CO}^{in}} \times 100 \quad (4)$$

$$X_{O_2}\ (\%) = \frac{n_{O_2}^{in} - n_{O_2}^{out}}{n_{O_2}^{in}} \times 100 \quad (5)$$

where n_{CO}^{in} and n_{CO}^{out} are the inlet and outlet CO (mol), respectively, and $n_{O_2}^{in}$ and $n_{O_2}^{out}$ are the O_2 counterparts.

The selectivity towards CO_2 was calculated by (Equation (6)):

$$sel_{CO_2}\ (\%) = \frac{1}{\lambda}\frac{X_{CO}}{X_{O_2}} \times 100 \quad (6)$$

where X_{CO} and X_{O_2} are the CO and O_2 conversions and λ is:

$$\lambda = 2 \times \frac{n_{O_2}^{in}}{n_{CO}^{in}} \quad (7)$$

The excess oxygen factor (λ) (Equation (2) used in this work was 2 considering that this value was previously found optimal for CO-PROX in previous research [24–27].

5. Conclusions

Several CuO-CeO_2 materials were synthesised by different synthetic methods (calcination of nitrate precursors, urea-nitrate combustion, freeze-drying, using poly (methyl metacrylate) spheres as templates, and precipitation methods using either NaOH or urea as a precipitating agent, with a nominal copper loading of 6 wt %. These CuO-CeO_2 catalysts were characterised and tested in the preferential oxidation of CO under an H_2-rich feed. All catalysts, except those synthesised from the urea combustion, displayed a quite high dispersion of copper and cerium oxides phases, as indicated by XRD and TEM measurements. The catalysts with smaller CeO_2 crystal size attained CO conversions between 90% and 100% at 115 °C, due to the existence of a higher number of CuO-CeO_2 interfacial sites, where the CO-PROX reaction takes place. In contrast, the larger CeO_2 crystal size of the sample synthesised by urea combustion gave rise to a lower number of available active sites, so the CO conversion was only 48% at 115 °C.

All catalysts showed high stability and selectivity even after 48 h TOS at 115 °C, obtaining CO conversion values close to 100%, with the system synthesised using PMMA microspheres as a template giving the highest value. In addition, the stability tests also discarded the deactivation by sintering or the modification of the active phases.

Among all the CuO-CeO_2 catalysts studied, those synthesised using PMMA showed excellent performance thanks to many concomitant factors, such as the very small CeO_2 particle size (5.6 nm), a surface rich in copper (atomic ratio Cu/Ce = 0.35), a higher proportion of Cu species more easily reducible (α peak 35.8%) and the high porosity of the material, as indicated by TEM micrography, which minimises the blockage of the active sites by H_2O in the stream. Furthermore, this catalyst

exhibits a very good CO conversion, close to 95%, under real operating conditions (10% H_2O, 15% CO_2) at 115 °C, which is within the working temperature range of a PEM fuel cell. This is higher than that reported in the literature for catalysts prepared by traditional synthetic strategies, which require a temperature between 170 and 200 °C for high CO conversion.

Supplementary Materials: The following are available online at www.mdpi.com/2073-4344/7/5/160/s1, Figure S1: Elemental mapping obtained by EDX for (**A**) F-D, (**B**) PMMA, (**C**) Na-Prec, (**D**) U-Prec, (**E**) N-Calc and (**F**) U-Comb catalysts.

Acknowledgments: The Spanish authors thank the Ministerio de Economía y Competitividad, Projects CTQ2015-68951-C3-3-R, MAT2013-42407, MAT2016-80933 and FEDER funds, Junta de Andalucía, Project P12-RNM-1565 and also to Fundación Cajacanarias for grant ENER02. Università Ca' Foscari Venezia is acknowledged by the Italian authors for the financial support.

Author Contributions: Juan Antonio Cecilia, Elisa Moretti, Pedro Núñez and Enrique Rodríguez-Castellón conceived and designed the experiments; Juan Antonio Cecilia and Ana Arango-Díaz performed the experiments; Juan Antonio Cecilia, Ana Arango-Díaz, Elisa Moretti and Loretta Storaro analysed the data; Juan Antonio Cecilia and Jaasiel Marrero-Jerez contributed reagents/materials/analysis tools; Juan Antonio Cecilia, Elisa Moretti and Enrique Rodríguez-Castellón wrote the paper.

Conflicts of Interest: The authors declare no conflict of interest.

References

1. Steele, B.C.H.; Heinzel, A. Materials for fuel-cell technologies. *Nature* **2001**, *414*, 345–352. [CrossRef] [PubMed]
2. Wu, J.; Yuan, X.Z.; Martin, J.J.; Wang, H.; Zhang, J.; Shen, J.; Wu, S.; Merida, W. A review of PEM fuel cell durability: Degradation mechanisms and mitigation strategies. *J. Power Sources* **2008**, *184*, 104–119. [CrossRef]
3. Moretti, E.; Storaro, L.; Talon, A.; Chitsazan, S.; Garbarino, G.; Busca, G.; Finocchio, E. Ceria-zirconia based catalysts for ethanol steam reforming. *Fuel* **2015**, *153*, 166–175. [CrossRef]
4. Palo, D.R.; Dagle, R.A.; Holladay, J.D. Methanol steam reforming for hydrogen production. *Chem. Rev.* **2007**, *107*, 3992–4021. [CrossRef] [PubMed]
5. Moretti, E.; Lenarda, M.; Storaro, L.; Frattini, R.; Patrono, P.; Pinzari, F. One-step incorporation of Pd-Zn catalytic sites into organized mesoporous alumina for use in the oxidative steam reforming of methanol. *J. Colloid Interface Sci.* **2007**, *306*, 89–95. [CrossRef] [PubMed]
6. O'Connell, M.; Kolb, G.; Schelhaas, K.; Schuerer, J.; Tiemann, D.; Ziogas, A.; Hessel, V. The development and evaluation of microstructured reactors for the water gas shift and preferential oxidation reactions in the 5 kW range. *Int. J. Hydrogen Energy* **2010**, *35*, 2317–2327. [CrossRef]
7. Trimm, D.L. Minimisation of carbon monoxide in a hydrogen stream for fuel cell application. *Appl. Catal. A* **2005**, *296*, 1–11. [CrossRef]
8. Jiménez, S.; Soler, J.; Valenzuela, R.X.; Daza, L. Assessment of the performance of a PEMFC in the presence of CO. *J. Power Sources* **2005**, *151*, 69–73. [CrossRef]
9. Lemons, R.A. Fuel cells for transportation. *J. Power Sources* **1990**, *29*, 251–264. [CrossRef]
10. Gray, P.G.; Frost, J.C. Impact on clean energy in road transportation. *Energy Fuels* **1998**, *12*, 1121–1129. [CrossRef]
11. Thomas, C.E.; James, B.D.; Lomax, F.D.; Kuhn, I.F. Fuel options for the fuel cell vehicle: Hydrogen, methanol or gasoline? *Int. J. Hydrogen Energy* **2000**, *25*, 551–567. [CrossRef]
12. Liu, K.; Wang, A.; Zhang, T. Recent advances in preferential oxidation of CO reaction over platinum group metal catalysts. *ACS Catal.* **2012**, *2*, 1165–1178. [CrossRef]
13. Guo, Z.; Liu, B.; Zhang, Q.; Deng, W.; Wang, W.; Wang, Y.; Yang, Y. Recent advances in heterogeneous selective oxidation catalysis for sustainable chemistry. *Chem. Soc. Rev.* **2014**, *43*, 3480–3524. [CrossRef] [PubMed]
14. Mishra, A.; Prasad, R. A review on preferential oxidation of carbon monoxide in hydrogen rich gases. *Bull. Chem. React. Eng. Catal.* **2011**, *6*, 1–14. [CrossRef]
15. Kipnis, M. Gold in CO oxidation and PROX: The role of reaction exothermicity and nanometer-scale particle size. *Appl. Catal. B* **2014**, *152*, 38–45. [CrossRef]

16. Rossignol, C.; Arrii, S.; Morfin, F.; Piccolo, L.; Caps, V.; Rousset, J.L. Selective oxidation of CO over model gold-based catalysts in the presence of H_2. *J. Catal.* **2005**, *230*, 476–483. [CrossRef]
17. Luengnaruemitchai, A.; Osuwan, S.; Gulari, E. Selective catalytic oxidation of CO in the presence of H_2 over gold catalyst. *Int. J. Hydrogen Energy* **2004**, *29*, 429–435. [CrossRef]
18. Zhang, Q.; Shore, L.; Farrauto, R.J. Selective CO oxidation over a commercial PROX monolith catalyst for hydrogen fuel cell applications. *Int. J. Hydrogen Energy* **2012**, *37*, 10874–10880. [CrossRef]
19. Gamarra, D.; Hornés, A.; Koppány, Z.; Schay, Z.; Munuera, G.; Soria, J.; Martínez-Arias, A. Catalytic processes during preferential oxidation of CO in H_2-rich streams over catalysts based on copper-ceria. *J. Power Sources* **2007**, *169*, 110–116. [CrossRef]
20. Martínez-Arias, A.; Hungría, A.B.; Munuera, G.; Gamarra, D. Preferential oxidation of CO in rich H_2 over CuO/CeO_2: Details of selectivity and deactivation under the reactant stream. *Appl. Catal. B* **2006**, *3*, 207–216. [CrossRef]
21. Avgouropoulos, G.; Ionnides, T. Selective CO oxidation over $CuO\text{-}CeO_2$ catalysts prepared via the urea-nitrate combustion method. *Appl. Catal. A* **2003**, *244*, 155–167. [CrossRef]
22. Ayastuy, J.L.; Gurbani, A.; González-Marcos, M.P.; Gutiérrez-Ortiz, M.A. Effect of copper loading on copper-ceria catalysts performance in CO selective oxidation for fuel cell applications. *Int. J. Hydrogen Energy* **2010**, *35*, 1232–1244. [CrossRef]
23. Caputo, T.; Lisi, L.; Pirone, R.; Russo, G. On the role of redox properties of CuO/CeO_2 catalysts in the preferential oxidation of CO in H_2-rich gases. *Appl. Catal. A* **2008**, *348*, 42–53. [CrossRef]
24. Arango-Díaz, A.; Cecilia, J.A.; Moretti, E.; Talon, A.; Núñez, P.; Marrero-Jerez, J.; Jiménez-Jiménez, J.; Jiménez-López, A.; Rodríguez-Castellón, E. Comparative study of CuO supported on CeO_2, $Ce_{0.8}Zr_{0.2}O_2$ and $Ce_{0.8}Al_{0.2}O_2$ based catalysts in the CO-PROX reaction. *Int. J. Hydrogen Energy* **2014**, *39*, 4102–4109. [CrossRef]
25. Arango-Díaz, A.; Cecilia, J.A.; dos Santos-Gómez, L.; Marrero-López, D.; Losilla, E.R.; Jiménez-Jiménez, J.; Rodríguez-Castellón, E. Characterization and performance in preferential oxidation of CO of $CuO\text{-}CeO_2$ catalysts synthesized using polymethyl metacrylate (PMMA) as template. *Int. J. Hydrogen Energy* **2015**, *40*, 11254–11260. [CrossRef]
26. Cecilia, J.A.; Arango-Díaz, A.; Rico-Pérez, V.; Bueno-López, A.; Rodríguez-Castellón, E. The influence of promoters (Zr, La, Tb, Pr) on the catalytic performance of $CuO\text{-}CeO_2$ systems for the preferential oxidation of CO in the presence of CO_2 and H_2O. *Catal. Today* **2015**, *253*, 115–125. [CrossRef]
27. Moretti, E.; Storaro, L.; Talon, A.; Lenarda, M.; Riello, P.; Frattini, R.; Martínez de Yuso, M.V.; Jiménez-López, A.; Rodríguez-Castellón, E.; Ternero, F.; et al. Effect of thermal treatments on the catalytic behaviour in the CO preferential oxidation of a $CuO\text{–}CeO_2\text{–}ZrO_2$ catalyst with a flower-like morphology. *Appl. Catal. B* **2011**, *102*, 627–637. [CrossRef]
28. Trovarelli, A.; Fornasiero, P. *Catalysts by Ceria and Related Materials*; Imperial College Press: London, UK, 2002.
29. Martínez-Arias, A.; Fernández-García, M.; Soria, J.; Conesa, J.C. Spectroscopic study of a Cu/CeO_2 catalyst subjected to redox treatments in carbon monoxide and oxygen. *J. Catal.* **1999**, *182*, 367–377. [CrossRef]
30. Maciel, C.G.; Silva, T.F.; Hirooka, M.I.; Belgacem, M.N.; Assaf, J.M. Effect of nature of ceria support in CuO/CeO_2 catalyst for PROX-Co reaction. *Fuel* **2012**, *97*, 245–252. [CrossRef]
31. Mishra, A.; Tripathi, B.D.; Rai, A.K.; Prasad, R. Comparative study of various preparation methods of $CuO\text{-}CeO_2$ catalysts for oxidation of *n*-hexane and iso-octane. *Bull. Chem. React. Eng. Catal.* **2013**, *7*, 172–178. [CrossRef]
32. Gurbani, A.; Ayastuy, J.L.; González-Marcos, M.P.; Gutiérrez-Ortiz, M.A. $CuO\text{-}CeO_2$ catalysts synthesized by various methods: Comparative study of redox properties. *Int. J. Hydrogen Energy* **2010**, *35*, 11582–11590. [CrossRef]
33. Moretti, E.; Lenarda, M.; Riello, P.; Storaro, L.; Talon, A.; Frattini, R.; Reyes-Carmona, A.; Jiménez-López, A.; Rodríguez-Castellón, E. Influence of synthesis parameters on the performance of CeO_2-CuO and $CeO_2\text{-}ZrO_2$-CuO systems in the catalytic oxidation of CO in excess of hydrogen. *Appl. Catal. B* **2013**, *129*, 556–565. [CrossRef]
34. Liu, Y.; Fu, Q.; Stephanopoulos, M.F. Preferential oxidation of CO in H_2 over $CuO\text{-}CeO_2$ catalysts. *Catal. Today* **2004**, *93*, 241–246. [CrossRef]

35. Barbato, P.S.; Colussi, S.; Di Benedetto, A.; Landi, G.; Lisi, L.; Llorca, J.; Trovarelli, A. Origin of high activity and selectivity of CuO/CeO_2 catalysts prepared by solution combustion synthesis in CO-PROX reaction. *J. Phys. Chem. C* **2016**, *120*, 13039–13048. [CrossRef]
36. Liu, B.; Liu, Y.; Hou, H.; Liu, Y.; Wang, Q.; Zhang, J. Variation of redox activity and synergistic effect for improving the preferential oxidation of CO in H_2-rich gases in porous Pt/CeO_2–Co_3O_4 catalysts. *Catal. Sci. Technol.* **2015**, *5*, 5139–5152. [CrossRef]
37. Liu, Z.; Zhou, R.; Zheng, X. Preferential oxidation of CO in excess hydrogen over CuO-CeO_2 catalyst prepared by chelating method. *J. Nat. Gas. Chem.* **2007**, *16*, 167–172. [CrossRef]
38. Yang, J.; Lukashuk, L.; Li, H.; Föttinger, K.; Rupprechter, G.; Schubert, U. High surface area ceria for CO oxidation prepared from cerium *t*-butoxide by combined sol–gel and solvothermal processing. *Catal. Lett.* **2014**, *144*, 403–412. [CrossRef] [PubMed]
39. Suzuki, K.; Sinha, A.K. Monodisperse, bimodal mesoporous ceria catalysts and adsorbents for air purification. *J. Mater. Chem.* **2007**, *17*, 2547–2551. [CrossRef]
40. Mariño, F.; Descorme, C.; Duprez, D. Supported based metal catalysts for the preferential oxidation of carbon monoxide in the presence of excess hydrogen (PROX). *Appl. Catal. B* **2005**, *58*, 175–183. [CrossRef]
41. Avgouropoulos, G.; Ioannides, T.; Matralis, M. Influence of the preparation method on the performance of CuO-CeO_2 catalysts for the selective oxidation of CO. *Appl. Catal. B* **2005**, *56*, 87–93. [CrossRef]
42. Avgouropoulos, G.; Ionnides, T. Effect of the synthesis parameters on catalytic properties of CuO-CeO_2. *Appl. Catal. B* **2006**, *67*, 1–11. [CrossRef]
43. Laguna, O.H.; Dominguez, M.I.; Oraá, S.; Navajas, A.; Arzamendi, G.; Gandía, L.M.; Centeno, M.A.; Montes, M.; Odriozola, J.A. Influence of the O_2/CO ratio and the presence of H_2O and CO_2 in the feed-stream during the preferential oxidation of CO (PROX) over a CuO_x/CeO_2 coated microchannel reactor. *Catal. Today* **2013**, *203*, 182–187. [CrossRef]
44. Gamarra, D.; Martínez-Arias, A. Preferential oxidation of CO in rich H_2 over CuO/CeO_2: Operando-DRIFTS analysis of deactivating effect of CO_2 and H_2O. *J. Catal.* **2009**, *263*, 189–195. [CrossRef]
45. Lee, H.C.; Kim, D.H. Kinetics of CO and H_2 oxidation over CuO-CeO_2 catalyst in H_2 mixtures with CO_2 and H_2O. *Catal. Today* **2008**, *132*, 109–116. [CrossRef]
46. Wu, Z.; Zhu, H.; Qin, Z.; Wang, H.; Ding, J.; Huang, L.; Wang, J. CO preferential oxidation in H_2-rich steam over a CuO/CeO_2 catalyst with high H_2O and CO_2 tolerance. *Fuel* **2013**, *104*, 41–45. [CrossRef]
47. Di Benedetto, A.; Landi, G.; Lisi, L.; Russo, G. Role of CO_2 on CO preferential oxidation over CuO/CeO_2 catalyst. *Appl. Catal. B* **2013**, *142–143*, 169–177. [CrossRef]
48. Williamson, G.K.; Hall, W.H. X-ray line broadening from filed aluminum and wolfram. *Metall. Acta* **1954**, *1*, 22–31. [CrossRef]
49. Konsolakis, M. The role of Copper-Ceria interactions in catalysis science: Recent theoretical and experimental advances. *Appl. Catal. B* **2016**, *198*, 49–66. [CrossRef]
50. Yao, S.Y.; Wu, W.Q.; Johnson-Peck, A.C.; Zhao, F.Z.; Liu, Z.Y.; Luo, S.; Senanayake, S.D.; Martínez-Arias, A.; Liu, W.J.; Rodriguez, J.A. Morphological effects of the nanostructured ceria support on the activity and stability of CuO/CeO_2 catalysts for the water-gas shift reactions. *Phys. Chem. Chem. Phys.* **2014**, *16*, 17183–17195. [CrossRef] [PubMed]
51. Spanier, J.E.; Robinson, R.D.; Zhang, F.; Chan, S.W.; Herman, I.P. Size-dependent properties of CeO_2-nanoparticles as studied by Raman scattering. *Phys. Rev. B* **2001**, *64*, 245407. [CrossRef]
52. Popovic, Z.; Dohcevic-Mitrovic, Z.; Konstantinovic, M.; Scepanovi, M. Raman scattering characterization of nanopowders and nanowires (rods). *J. Raman Spectrosc.* **2007**, *38*, 750–755. [CrossRef]
53. Shan, W.J.; Feng, Z.C.; Li, Z.I.; Jing, Z.; Shen, W.J.; Can, L. Oxidative steam reforming of methanol on $CeO_{0.9}Cu_{0.1}O_Y$ catalysts prepared by deposition-precipitation, and complexation-combustion methods. *J. Catal.* **2004**, *228*, 206–217. [CrossRef]
54. Thommes, M.; Kaneko, K.; Neimark, A.V.; Olivier, J.P.; Rodríguez-Reinoso, F.; Roquerol, J.; Sing, K.S.W. Physisorption of gases, with special reference to the evaluation of surface area and pores size distribution (IUPAC Technical Report). *Pure Appl. Chem.* **2015**, *87*, 1051–1069. [CrossRef]
55. Marbán, G.; Fuentes, A.B. Highly active and selective CuO_x/CeO_2 catalyst prepared by a single-step citrate method for preferential oxidation of carbon monoxide. *Appl. Catal. B* **2005**, *57*, 43–53. [CrossRef]
56. Rao, K.N.; Venkataswamy, P.; Reddy, B.M. Structural characterization and catalytic evaluation of supported copper-ceria catalysts for soot oxidation. *Ind. Eng. Chem. Res.* **2011**, *50*, 11960–11969. [CrossRef]

57. Senanayake, S.D.; Rodríguez, J.A.; Stacchiola, D. Electronic metal-support interactions and the production of hydrogen through the water-gas shift reactions and ethanol steam reforming: Fundamental studies with well-defined model catalyst. *Top. Catal.* **2013**, *53*, 1488–1498. [CrossRef]
58. Hu, P.; Huang, Z.; Amghouz, Z.; Makkee, M.; Xu, F.; Kapteijn, F.; Dikhtiarenko, A.; Chen, Y.; Gu, X.; Tang, X. Electronic metal-support interactions in single-atoms catalysts. *Angew. Chem. Int. Ed.* **2014**, *53*, 3418–3421. [CrossRef] [PubMed]
59. Lu, Z.; Yang, Z.; He, B.; Castleton, C.; Hermansson, K. Cu-doped ceria oxygen vacancy formation made easy. *Chem. Phys. Lett.* **2011**, *510*, 60–66. [CrossRef]
60. Zhang, F.; Wang, P.; Koberstein, J.; Khalid, S.; Chan, S. Cerium oxidation state in ceria nanoparticles studied with X-ray photoelectron spectroscopy and absorption near edge spectroscopy. *Surf. Sci.* **2004**, *563*, 74–82. [CrossRef]
61. Konsolakis, M.; Carabineiro, S.A.C.; Papista, E.; Marnellos, G.E.; Tavares, P.B.; Moreira, J.A.; Romaguera-Barcelay, Y.; Figuereido, J.L. Effect of the preparation method on the solid state properties and the deN_2O performance of CuO-CeO_2 oxides. *Catal. Sci. Technol.* **2015**, *5*, 3714–3727. [CrossRef]
62. Arango-Díaz, A.; Moretti, E.; Talon, A.; Storaro, L.; Lenarda, M.; Núñez, P.; Marrero-Jerez, J.; Jiménez-Jiménez, J.; Jiménez-López, A.; Rodríguez-Castellón, E. Preferential CO oxidation (CO-PROX) catalyzed by CuO supported on nanocrystalline CeO_2 prepared by a freeze-drying method. *Appl. Catal. A* **2014**, *477*, 54–63. [CrossRef]
63. Martínez-Arias, A.; Gamarra, D.; Hungría, A.B.; Fernández-García, M.; Munuera, G.; Hornés, A.; Bera, P.; Conesa, J.C.; López-Cámara, A. Characterization of active sites/entities and redox/catalytic correlations in copper-ceria-based catalysts for preferential oxidation of CO in H_2-rich streams. *Catalysts* **2013**, *3*, 378–400. [CrossRef]
64. Cecilia, J.A.; Arango-Díaz, A.; Franco, F.; Jiménez-Jiménez, J.; Storaro, L.; Moretti, E.; Rodríguez-Castellón, E. CuO-CeO_2 supported on montmorillonite-derived porous clay heterostructures (PCH) for preferential CO oxidation in H_2-rich stream. *Catal. Today* **2015**, *253*, 126–136. [CrossRef]
65. Zou, D.; Aklonis, J.J.; Salovey, R. Model filled polymers. Synthesis of monodisperse crosslinked polymethacrylonitrile beads. *J. Polym. Sci. Part A* **1992**, *30*, 2443–2449. [CrossRef]
66. Jiménez-Gómez, C.P.; Cecilia, J.A.; Márquez-Rodríguez, I.; Moreno-Tost, R.; Santamaría-González, J.; Mérida-Robles, J.; Maireles-Torres, P. Gas-phase hydrogenation of furfural over Cu/CeO_2 catalysts. *Catal. Today* **2017**, *279*, 327–338. [CrossRef]
67. Brunauer, S.; Emmett, P.H.; Teller, E. Adsorption of gases in multimolecular layers. *J. Am. Chem. Soc.* **1938**, *60*, 309–319. [CrossRef]